Young S. Kwon[1] *and Bhavani V. Sankar*[1]

Indentation-Flexure and Low-Velocity Impact Damage in Graphite Epoxy Laminates

REFERENCE: Kwon, Y. S. and Sankar, B. V., "Indentation-Flexure and Low-Velocity Impact Damage in Graphite Epoxy Laminates," *Journal of Composites Technology & Research*, JCTRER, Vol. 15, No. 2, Summer 1993, pp. 101–111.

ABSTRACT: Static indentation-flexure and low-velocity impact tests were performed on quasi-isotropic and cross-ply graphite/epoxy composite laminates. The load-deflection relations in static tests and impact force history in impact tests were recorded. The damage was assessed by using ultrasonic C-scanning and photo-micrographic techniques. Some features of the static behavior were explained by simple analytical models. A good correlation existed between the load-deflection curves for static and impact loading. It was found that results from a few static indentation-flexure tests can be used to predict the impact force history and delamination radius in composite laminates due to low-velocity impact.

KEYWORDS: indentation damage, impact damage, composite laminates, graphite/epoxy, delamination

Composite laminates are very susceptible to impact damage during handling or service. Often the impact damage is in the form of matrix cracks and delaminations, which are hard to detect. The major goal of our research is to develop an analytical/numerical methodology to predict impact damage, given the description of the impactor and the target.

In the present study we focus our attention on a class of impact problems where the impact mass is very large, e.g., 1 to 15 kg, and the impact velocity is very low, e.g., 0 to 3 m/s. Such impacts are typical of handling damage and dropping of objects on composite structures. Previous analytical studies [*1*] have shown that for large mass, low-velocity impact, the impact duration is several orders of magnitude higher than the time for the flexural waves to travel to the boundaries of the target, and hence the impact event can be considered as quasi-static.

In this study a series of static indentation-flexure tests was performed using different types of laminates made of graphite/epoxy composite. The load-deflection relations were recorded. The damage was assessed by ultrasonic C-scanning and also using photo-micrography. Some features of the static load-deflection curves are explained by simple analytical models. Impact tests were performed, and the damage was quantified using similar techniques. The relation between static and dynamic responses was examined. A model for predicting the low-velocity impact response and delamination radius based on the static test results is proposed.

[1]Graduate student and associate professor, respectively, Department of Aerospace Engineering, Mechanics and Engineering Science, University of Florida, Gainesville, FL 32611–2031.

Materials and Methods

The graphite/epoxy laminated plates were fabricated from 305-mm-wide Hercules AS4/3501-6 prepreg tapes in an autoclave. Three types of laminates were fabricated: Type A is $\pi/8$ quasi-isotropic laminate $[0,22.5,45,67.5,-45,-22.5]_{2s}$; Type B is cross-ply laminate $[0,90]_{8s}$; and Type C is $\pi/4$ quasi-isotropic laminate $[0,45,90,-45]_{4s}$. The average thickness of the plates was 3.8 mm. The properties of the composite material were measured using ASTM standard tests [*2*]. The sides of the square specimens were about an inch longer than the diameter of the circular support rings used in the indentation-flexure and impact tests. Hence the specimens can be considered as simply supported circular plates. The support ring diameters were 50.8 mm, 76.2 mm, and 101.6 mm. The two steel indenters had hemispherical noses of diameters 6.35 mm and 25.4 mm, respectively.

The indentation test setup consisted of the following loading apparatus, recording devices, and data processing devices [*2*]: MTS material testing machine, digital oscilloscope (Nicolet 4094), Nicolet XF-44 recorder, LVDT (Schaevitz model 500 MHR), analog transducer amplifier (Schaevitz model ATA-101), specimen support fixture, and a microcomputer. A schematic of the test setup is shown in Fig. 1. The tests were conducted under stroke control at the rate of 0.02 mm/s. The load and plate center deflection data were acquired at the rate of 5 samples/second and were recorded by the Nicolet XF-44 recorder. The data were transferred to a microcomputer from the oscilloscope and were processed in the microcomputer. After indentation tests the specimens were C-scanned to map the delamination areas.

Low-velocity impact tests were conducted on composite laminates in order to compare the response and damage with corresponding behavior under static loading. The laminate types, indenters, and support ring diameters were the same as used in static tests. The impact equipment depicted in Fig. 2 is a modified version of the one used in Ref *3*, and consists of an impact pendulum hung from the laboratory ceiling, an impact tup (Dynatup 8496-1), a strain gage conditioner (Vishay 2310), a digital oscilloscope and recorder (Nicolet 4094 and XF-44), and a microcomputer. The impact history was accessed by the oscilloscope and was recorded by the recorder. The impact and rebound velocities were measured using two pairs of photo transistors and light-emitting diodes with two 10-MHz counters. From the ex-

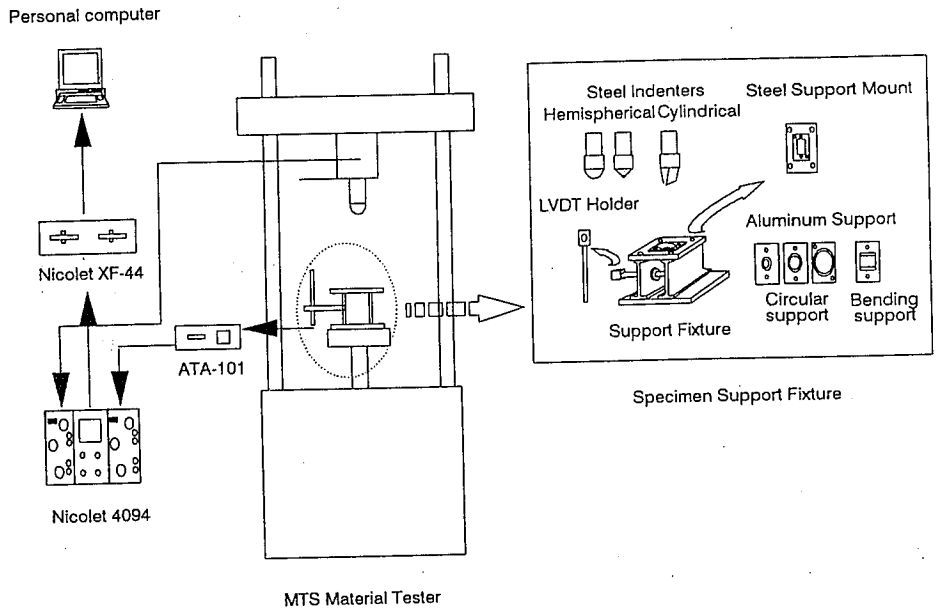

FIG. 1—*Schematic of static indentation test setup.*

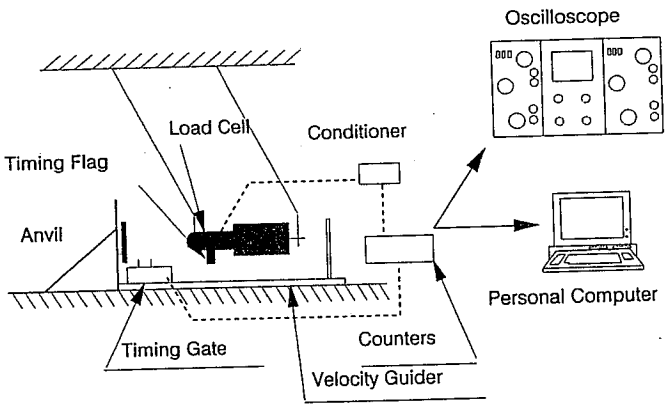

FIG. 2—*Schematic of impact pendulum setup.*

perimentally measured impact force history, and the impact velocity, a relation between the contact force and impactor displacement can be derived by integrating the equation of motion of the impactor. A detailed description of the impact tests can be found in Ref 2.

Results and Discussion of Static Tests

The load-deflection diagrams of all the indentation-flexure tests are presented in Ref 2. Some plots are presented in Figs. 3 through 5 for the purpose of discussion. The general observations about the indentation damage and effects of layup, plate diameter, and indenter diameter are discussed in the following section. It should be mentioned that the deflection is actually the displacement of the indenter or the impactor, which is the sum of the plate deflection and the local indentation.

Some General Observations

There are some common features in the load-deflection diagrams of the three types of laminates A, B, and C. Referring to Fig. 3, the initial portion of the loading curve OA shows some nonlinearity, which can be attributed to local Hertzian type indentation. As the load is increased, the plate deflection becomes much larger than the amount of indentation, and the load-deflection curve is almost linear (AB in Fig. 3). One could hear intermittent crackling noise, typical of matrix cracking, but no apparent stiffness loss was observed during this stage. When the load reached a critical value, denoted by D in Fig. 3, there was a sudden load drop. The noise level and the amount of load drop associated with the failure were highest for the cross-ply laminates (Type B), lowest in the $\pi/8$ quasi-isotropic laminates (Type A), and intermediate in the $\pi/4$ quasi-isotropic laminates (Type C). It is suspected that the load drop is caused by unstable propagation of delaminations. A comparison of failures in different types of laminates is presented in Fig. 4.

After the first observable failure, there is a significant loss of plate stiffness denoted by the reduced slope of the subsequent unloading and reloading curves, e.g., FG and GF, HJ and JH, etc. in Fig. 3. As will be seen later, the delaminations grow in a stable manner as the load is increased. The loading curve EFHK, which represents delamination growth (similar to yielding in ductile materials), will be called the D-curve (damage accumulation curve). The D-curve is almost a straight line until the center deflection is about 3 mm (note that the average plate thickness is 3.8 mm). Thereafter there is a sudden increase in the slope of the D-curve as observed in Fig. 4. The slopes of the unloading curves at this stage are sometimes greater than the stiffness of the undamaged plate and were highly nonlinear also. The nonlinearity can be attributed to (a) large deflection of the plate; (b) membrane action in the delaminated plies; and (c) friction between various contacting surfaces, e.g., between the indenter and the plate, between delaminations, and between the plate and the support.

Some specimens were unloaded even before the first observable failure (BC in Fig. 3), and there were some energy losses indicated by the hysteresis loop (area OBC). This energy loss can be attributed mainly to material damage, and to some extent to friction at contact areas. When unloaded at higher loads, the

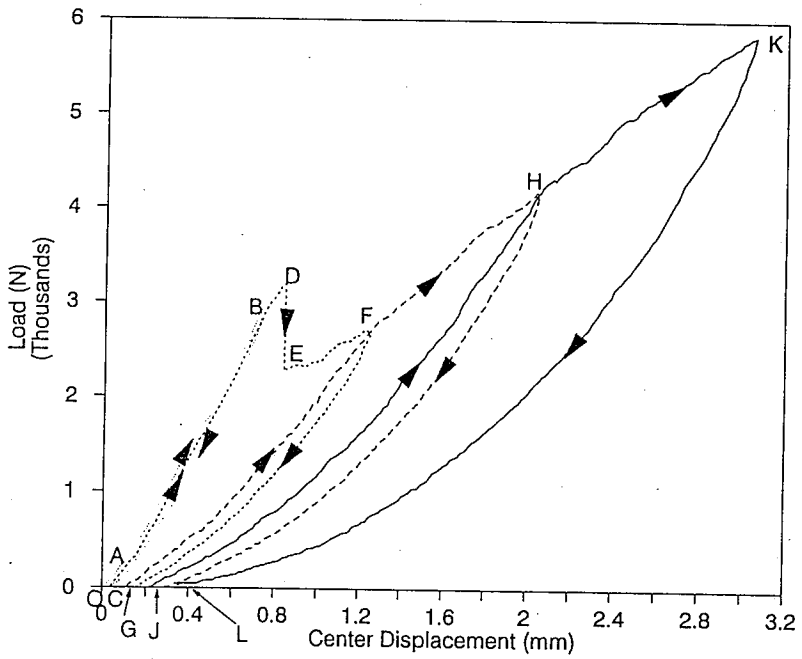

FIG. 3—*Typical load-deflection curve for graphite/epoxy laminates.*

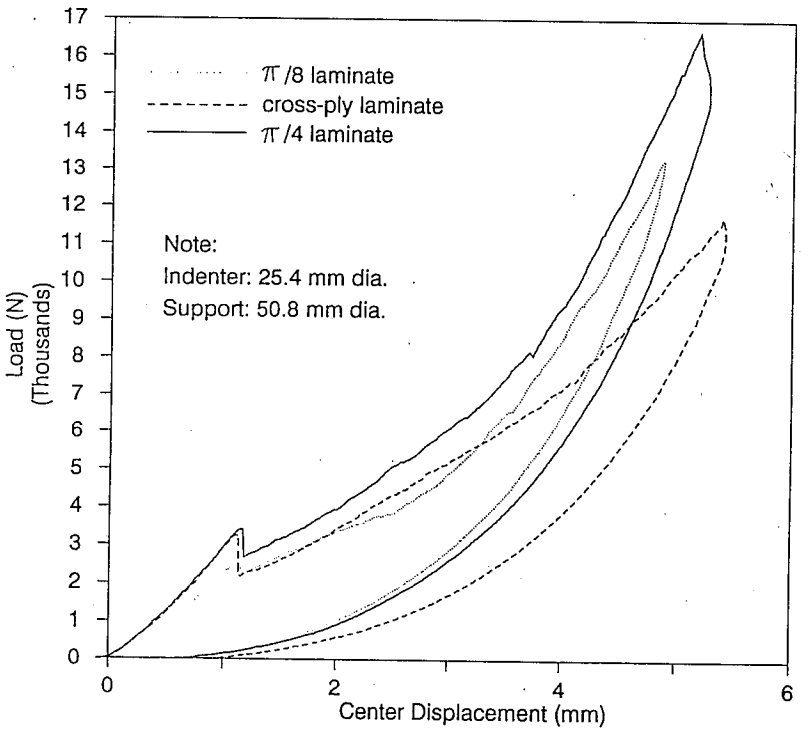

FIG. 4—*Static load-deflection curves for various types of laminates.*

unloading and reloading curves were highly nonlinear (e.g., FG and GF, HJ, and JH). The area between the corresponding unloading and reloading curves, e.g., FG and GF, is the measure of frictional energy dissipation. The area between an unloading curve and the next reloading curve, e.g., FG and JH, is an example of energy dissipation due to material damage, mostly delaminations.

There were no significant visible damages either on the front surface or back surface even when the loads were as high as 10 000 N. The indenter always left a small dent at the point of contact. A sketch of a typical load-deflection curve is shown in Fig. 5. This sketch will be used for the purpose of discussion of results in the following sections.

Loading up to Initial Observable Failure

Except for the initial nonlinear contact behavior, the loading curve can be considered almost linear. The area between the

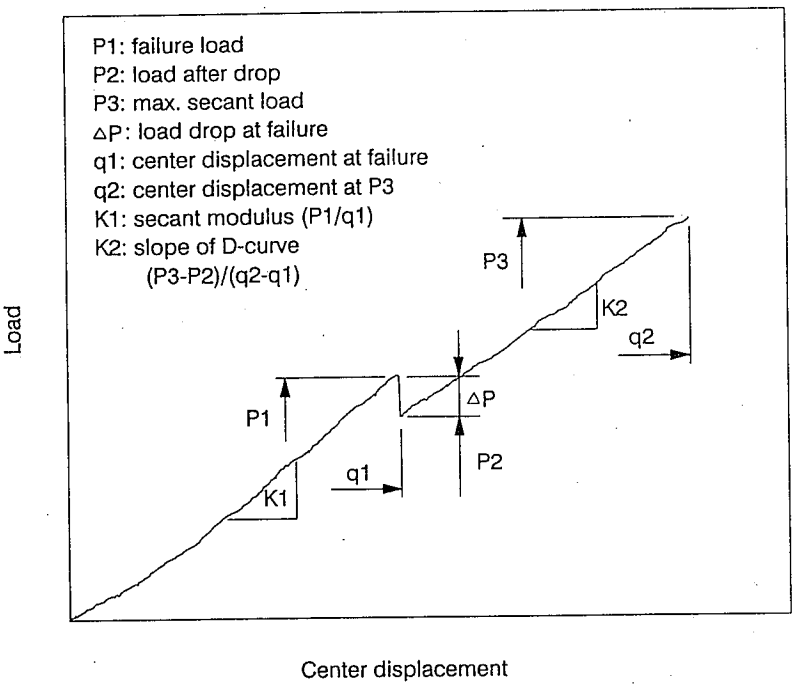

FIG. 5—*Sketch of load-deflection relation.*

loading and unloading curves in this figure represents energy dissipation due to formation of microcracks and some frictional effects. Figure 6 depicts the failure load P_1 for the initial observable damage for different types of laminates, different diameter support rings, and the two indenters (see Fig. 5 for the definition of P_1). For each combination of test parameters three repeat tests were performed. For all cases shown, the failure load due to 25.4-mm-diameter indenter was about 30% higher than that for 6.35-mm-diameter indenter. The only explanation seems to be that for a given load the contact radius is proportional to the cube root of the indenter radius [*4*], and hence the contact pressure will be less for a given load in the case of larger indenter. This may have an effect on the load at which matrix cracks initiate a delamination in the plate.

In all cases (Fig. 6), Type A ($\pi/8$) laminates failed at significantly lower loads compared to the B and C Types. The Type C laminates ($\pi/4$) performed better than the cross-ply laminates (Type B) under the 50.8-mm ring support, but failed at slightly lower loads under 76.2- and 101.6-mm supports. The center deflections at the instant of failure are presented in Fig. 7. It should be reminded that the center deflection is the displacement of the indenter, which includes both the flexural deflection and local indentation. It is interesting to see that for a given support ring size, the center deflection at failure does not depend on the indenter diameter very much. In fact, the indenter diameter will affect the local contact stresses for a given load, which may in turn affect the local damage. However, the plate stresses are expected to govern the damage growth as the damage progresses outward. This could be a possible explanation for the good correlation between the center deflection and the damage irrespective of the indenter diameter.

After the unstable failure, there is a significant load drop in the displacement controlled tests. The load drops for different sets of test parameters are shown in Fig. 8. In general, the load drop is higher if the failure load is higher. The $\pi/8$ laminates do not show much load drop. It was observed that the failure in $\pi/8$ laminates was not sudden as in the other two types during the tests, but a gradual growth of damage was observed. The load drop in the case of cross-ply laminates is in general higher than for the $\pi/4$ quasi-isotropic laminates.

As the loading continues, the delaminations caused by the initial failure continue to grow in a stable manner. Before we discuss the unloading and reloading tests, it will be instructive to look at the ultrasonic C-scan results.

Ultrasonic C-Scan Results

The damaged specimens were C-scanned to map the area of delamination. The damage pattern was almost circular in all cases. It should be noted that the C-scan provides the projected area of the damage whereas the actual damage is a "staircase type" delamination as mentioned in Ref 7. This may be because of the quasi-isotropic nature of the laminates and the circular support used in the tests. In Fig. 9 the delamination radii are plotted against the maximum contact force applied during the test for $\pi/4$ laminates (Type C). In the case of Type C laminates the delamination radius was directly proportional to the maximum load irrespective of the indenter size or the plate size. A linear relation between the delamination radius and the maximum load was obtained using least square curve fitting. There was some scatter in the data for Type A and Type B laminates as seen in Figs. 10 and 11. However, it was decided to use a linear fit for all the results. The delamination radius b can be expressed as $b = BP_{max}$, where B is the constant of proportionality. The constant B in mm/N units for the $\pi/8$, cross-ply, and $\pi/4$ laminates, respectively, were found as 0.005295, 0.004334, and 0.003863 for static loading. Thus one can see that $\pi/4$ laminates have better delamination resistance than cross-ply laminates, and cross-ply laminates are better than $\pi/8$ laminates.

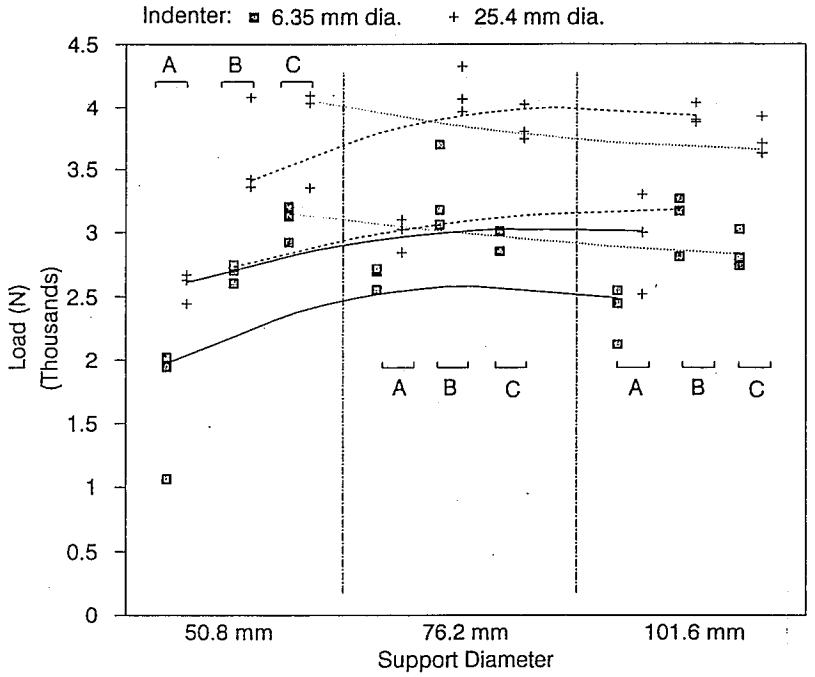

Note:
A: $\pi/8$ laminate
B: cross-ply laminate
C: $\pi/4$ laminate

FIG. 6—*Failure load* (P_1) *for laminate types of* $\pi/8$, *cross-ply and* $\pi/4$.

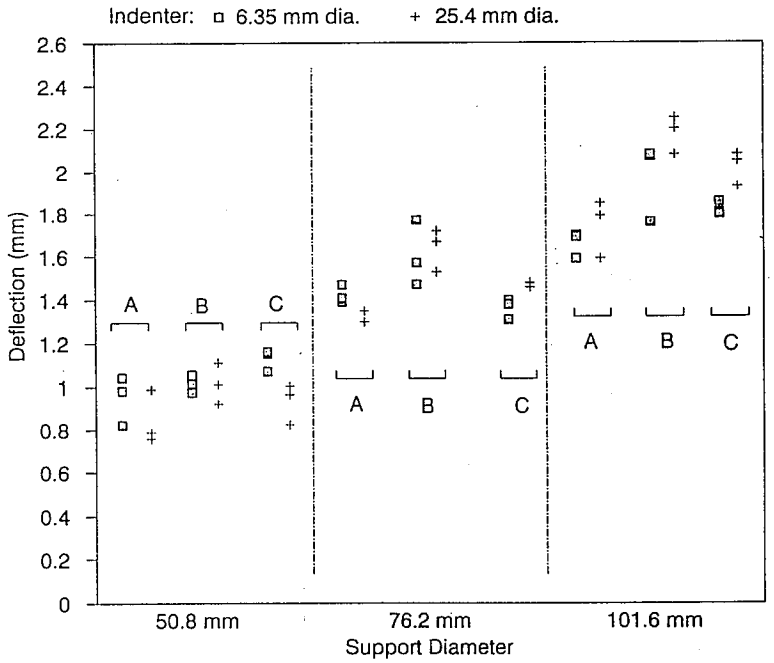

Note:
A: $\pi/8$ laminate
B: cross-ply laminate
C: $\pi/4$ laminate

FIG. 7—*Center deflection* (q_1) *at failure.*

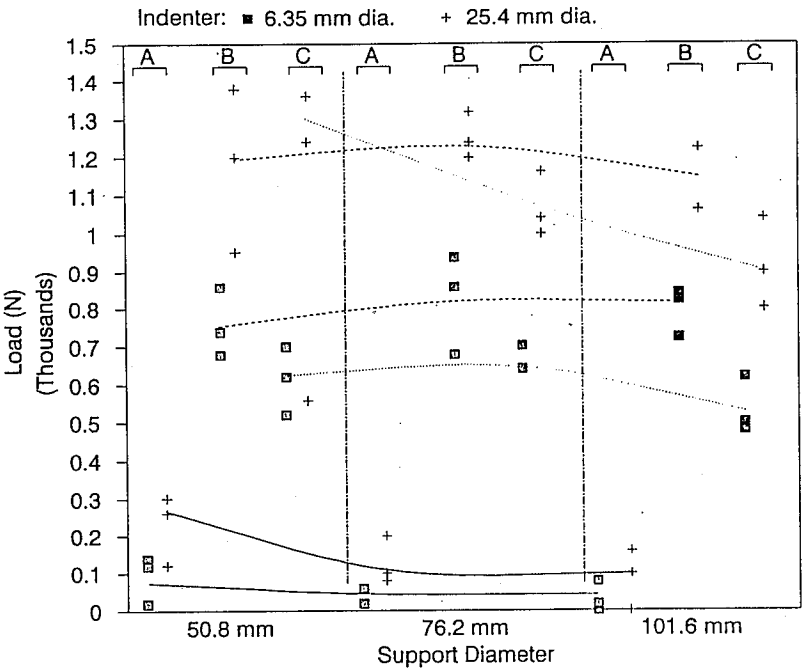

Note:

A: $\pi/8$ laminate
B: cross-ply laminate
C: $\pi/4$ laminate

FIG. 8—*Load drop(ΔP) at failure.*

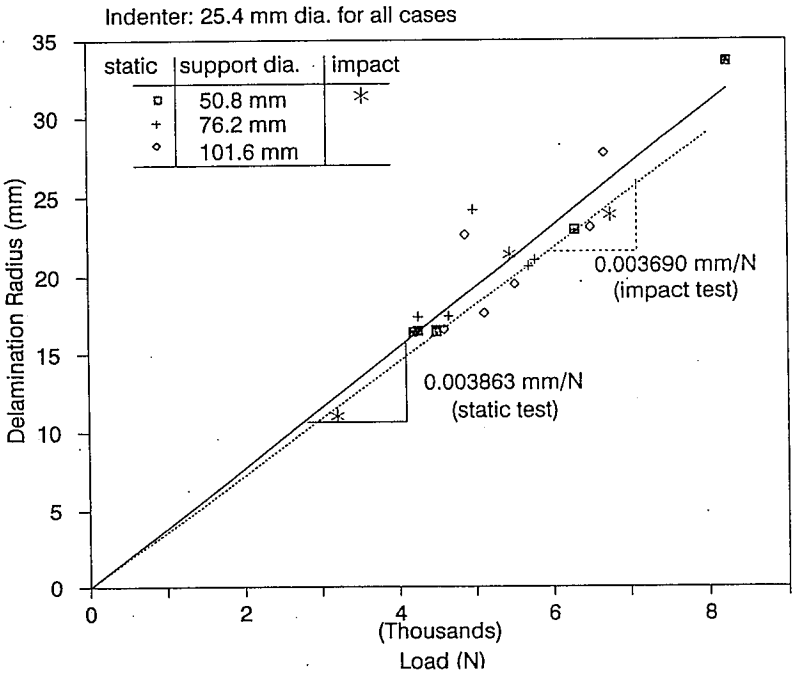

FIG. 9—*Delamination radius versus maximum load for π/4 type laminate.*

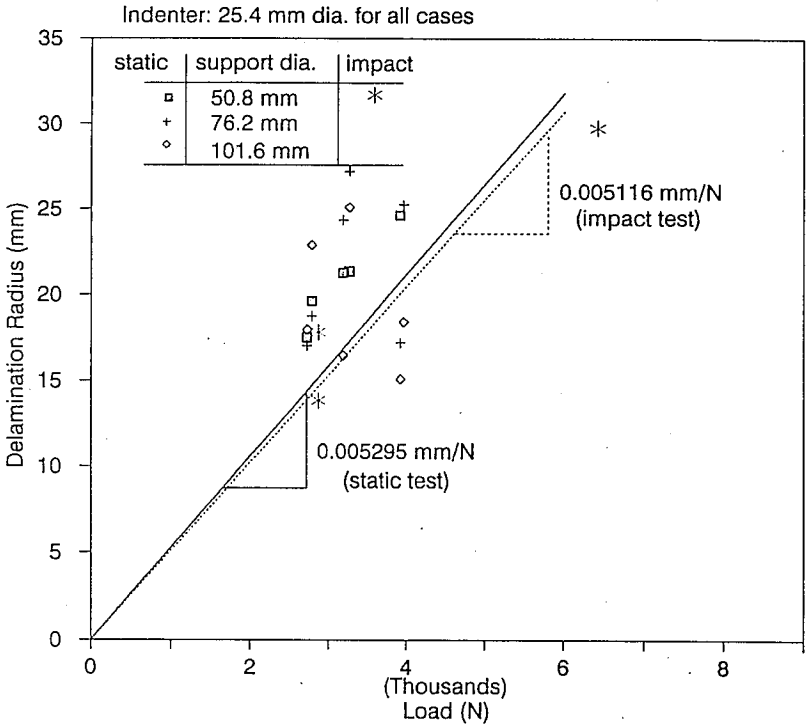

FIG. 10—*Delamination radius versus maximum load for π/8 type laminate.*

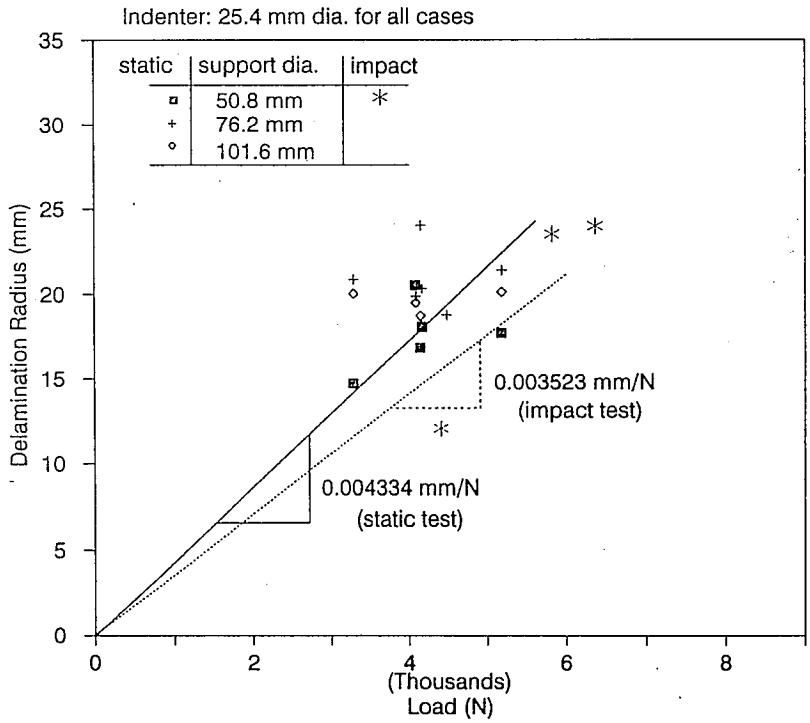

FIG. 11—*Delamination radius versus maximum load for cross-ply laminate.*

Loading, Unloading, and Reloading Curves

The discussion in this section pertains to loading after the initial observable load drop. As the loading continues, the delamination also grows in a stable manner. The unloading curves are highly nonlinear (Fig. 3). The stiffness is higher at the instant of unloading and gradually decreases as the load is reduced. When reloaded the load-deflection is again nonlinear with stiffness increasing as the load is increased. The nonlinear load-deflection behavior is largely due to the membrane action of the delaminated plies [5,6]. The area formed by the unloading and reloading curves represents the energy dissipated by friction between contacting surfaces.

Fractographic Studies

The plates damaged by indentation-flexure tests were sectioned along a diametrical plane, polished, and observed in an optical microscope. Three specimens, one for each laminate type, were selected. In each specimen the loading was stopped immediately after the first observable load drop. A fourth specimen was Type C laminate in which loading was stopped just before the anticipated sudden failure. The schematic diagrams of delaminations are shown in Fig. 12. As seen from Fig. 12*d*, there are delaminations even before the sudden load drop occurs. That substantiates the conclusion that the crackling noise heard during loading was due to both matrix cracking and initiation of small delaminations. The load drop and the associated *bang* are due to connecting of various delaminations and unstable delamination propagation. It should be mentioned that the delamination patterns were not strictly axisymmetric. We were able to observe the spiralling staircase type damage pattern as reported in Ref 7. There were no delaminations in the top portion of the laminates. The envelope of delamination fronts in all the layers resembled a conical tent. A simple plate model is presented in the next section to support this observation.

Analytical Models

In this section we derive some analytical models to qualitatively explain the delamination patterns observed in static tests and also to predict the impact force history and delamination radius due to the impact.

Delamination Pattern in Static Tests

We assume that the delaminations initiate from the tips of matrix cracks, and the maximum tensile stresses in the matrix are responsible for the matrix cracks. Even though we need to perform a detailed analysis to obtain the matrix stresses in a laminated plate, a quick understanding of the nature of their variation can be obtained by considering the plate as homogeneous. For a given layup the actual matrix stresses will be proportional to the average stresses obtained from the homogeneous plate model. The expressions for the normal and the shear stresses in a simply supported circular plate subjected to a central load are [8]

$$\sigma_{rr} = \frac{12z}{h^3} M_r \tag{1a}$$

$$\sigma_{\theta\theta} = \frac{12z}{h^3} M_t \tag{1b}$$

$$\tau_{rz} = \frac{1.5P}{2\pi rh}\left[\frac{h^2}{4} - z^2\right] \tag{1c}$$

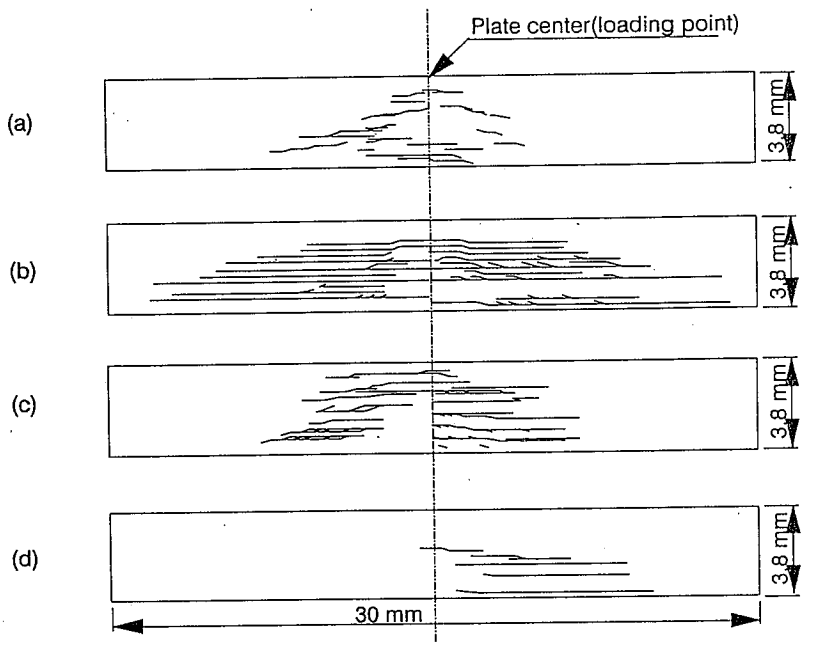

FIG. 12—*Schematics of delaminations and matrix cracks:* (a) $\pi/8$ *laminate;* (b) *cross-ply laminate;* (c) $\pi/4$ *laminate; and* (d) $\pi/4$ *laminate. Cases*(a-c): *after initial load drop; Case*(d): *before load drop.*

where the bending moments, M_r and M_t, are

$$M_r = \frac{P}{4\pi}(1 + \nu)\log\frac{a}{r} \tag{2a}$$

$$M_t = \frac{P}{4\pi}\left[(1 + \nu)\log\frac{a}{r} + 1 - \nu\right] \tag{2b}$$

In these expressions P is the central load, a is the plate radius, and ν is the Poisson's ratio, which is assumed to be equal to 0.3 for the purpose of illustration. In the axisymmetric plate $\sigma_{\theta\theta}$ is one of the principal stresses. The other two principal stresses are given by

$$\sigma_1 = \frac{\sigma_{rr}}{2} + \sqrt{\left(\frac{\sigma_{rr}}{2}\right)^2 + \tau_{rz}^2} \tag{3a}$$

$$\sigma_2 = \frac{\sigma_{rr}}{2} - \sqrt{\left(\frac{\sigma_{rr}}{2}\right)^2 + \tau_{rz}^2} \tag{3b}$$

The contour of constant σ_1 and $\sigma_{\theta\theta}$ for a unit load are shown in Figs. 13 and 14. The principal stress σ_2 is mostly compressive and hence not presented. Referring to the delamination patterns

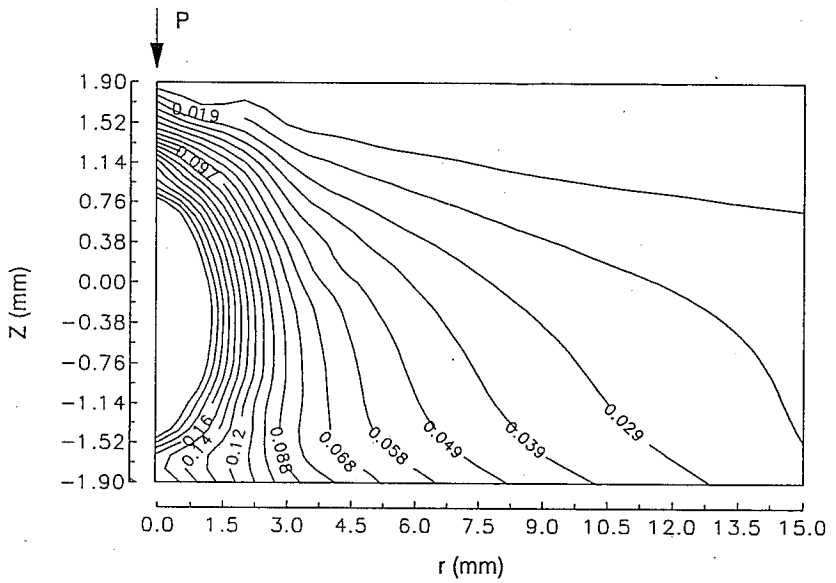

FIG. 13—*Contour plot of tensile principal stress (σ_1) for a unit load.*

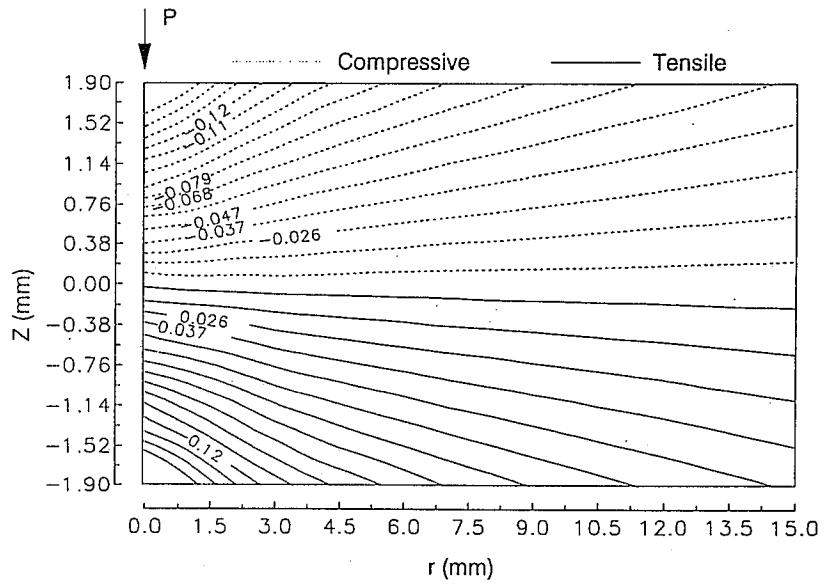

FIG. 14—*Contour plot of principal stress ($\sigma_{\theta\theta}$) for a unit load.*

shown in Fig. 12, one can note that the envelope of the delamination fronts (which resembles a conical tent) is similar to the iso-principal stress curves. This suggests that the tensile principal stresses may govern the initiation of microcracks and hence delaminations. The subsequent growth of delaminations may be governed by their initial radius and location along the thickness. For example, a finite element analysis by Pinheiro [9] shows that the strain energy release rate is higher for delaminations at the midplane of a laminated beam than that at other positions.

Prediction of Impact Response and Damage

It has been found that for all the impact tests we conducted, the load-deflection relations were similar to the ones for the corresponding static tests [2]. Hence the static load-deflection relations can be used to model the impact response. A typical static curve (e.g., Fig. 5) can be modeled by three empirical formulas. For the initial loading portion up to the first observable load drop, the load-deflection relation can be expressed as

$$P = K_1 q, q < q_1 \tag{4}$$

where P is the contact force, q is the plate deflection, K_1 is the slope of the static curve, and q_1 is the deflection at which load drop ΔP occurs. After the load drop, the load-deflection follows the D-curve given by

$$P = (K_1 q_1 - \Delta P) + K_2 (q - q_1), q > q_1 \tag{5}$$

This relation is valid as long as the load is increasing. Once the unloading begins, i.e., contact force starts decreasing, the load-deflection follows the unloading curve approximated as a parabola (see Fig. 3) given by

$$P = P_{max} \left(\frac{q}{q_{max}} \right)^2 \tag{6}$$

where P_{max} and q_{max} are the load and deflection at the point of unloading. In fact, the exponent in Eq 6 can be accurately estimated by curve fitting the static unloading curves. This formula neglects the residual deformation at the end of the contact/impact process. In fact, the unloading process is not critical in estimating the maximum impact force. The equation of motion of the impactor is given by

$$M\ddot{q} = -P(q) \tag{7}$$

where M is the impactor mass and $\ddot{q}$ is the acceleration. The force function $P(q)$ is chosen from Eqs 4 through 6 depending on the contact force and deflection. The equation of motion can be numerically integrated to obtain force-time history. The constants K_1, q_1, ΔP, and K_2 are obtained from one simple static test. The previous procedure was tried for several impact tests and the agreement between the measured and predicted impact response, in particular the maximum contact force, was excellent [2]. A sample comparison is shown in Fig. 15. The numerical values used were: K_1 = 4065.4 N/mm, q_1 = 0.94 mm, ΔP = 1300 N, and K_2 = 2184 N/mm. Now from the maximum predicted contact force, one can predict the delamination radius using the C-scan results for the static tests. The delamination radius obtained using C-scan for impact tests on Type C laminates is plotted in Fig. 8 along with corresponding static results. For a given maximum contact force, the delamination radius in impact tests is slightly smaller than in static tests. Thus static tests provide a conservative estimate of the delamination radius for the quasi-static impact regime.

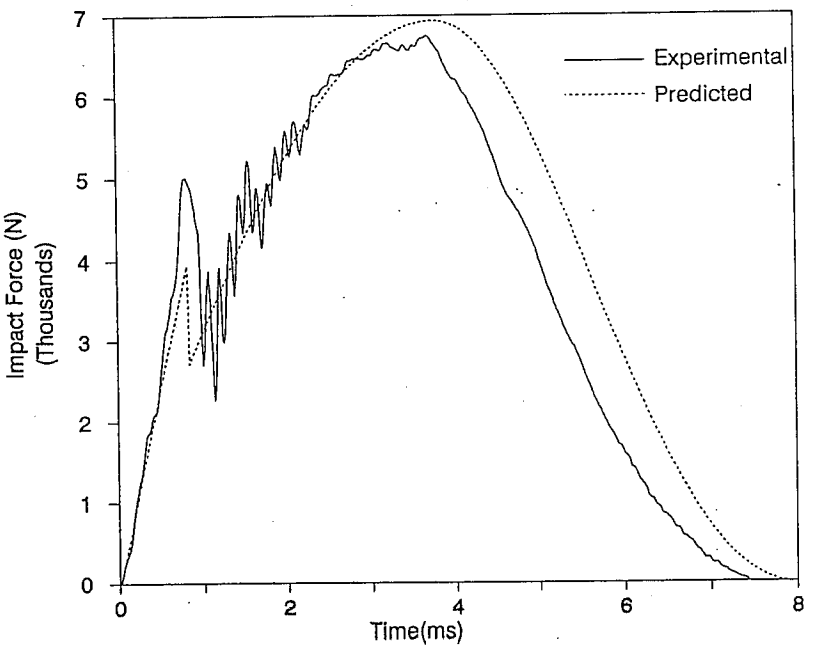

FIG. 15—*Impact force history for π/4 laminate: Impactor mass–13.98 kg; impact velocity–1.27 m/s.*

Conclusions

Static indentation-flexure and low-velocity impact tests were conducted on simply supported circular graphite/epoxy laminated plates. Indenters of two different radii, three laminate configurations, and three different plate radii were considered. In static tests matrix cracks and small delaminations were observed before the sudden failure which was caused by enlarged delaminations. Upon further loading, the delaminations continue to grow steadily. The traditional $\pi/4$ quasi-isotropic laminates performed better than the $\pi/8$ and the cross-ply laminates of the same thickness in the sense that they withstood large forces before the unstable failure. However, the $\pi/8$ laminates failed at lower loads, exhibiting a gradual growth of damage, which may be desirable in some applications. The experimental data collected thus far will be very useful in detailed finite element modeling of the static tests and in identifying the mechanisms responsible for matrix cracking and delamination initiation. The load-deflection behavior in impact tests is very similar to the corresponding static behavior before and after damage. Hence the static response curves were used to predict damage due to large impact masses at very low velocities. From the load-deflection diagrams and the extent of damage obtained from very few static indentation-flexure tests, and with the impact analysis program [1], it will now be possible to predict impact damage in similar specimens for several combinations of impact masses and velocities.

Acknowledgments

This research was supported by the NASA Langley Research Center Grant NAG-1-826 to the University of Florida. The authors thank Mr. C. C. Poe, Jr., the contract monitor, for his support and many helpful discussions. Thanks are also due to Mr. M. A. Portanova, NASA Langley Research Center, for his help in ultrasonic C-scanning of the specimens.

References

[1] Sankar, B. V., Ku, C., and Nguyen, P. T., "Nondimensional Impact Models for Composite Laminates," in *Proceedings of the 5th Technical Conference*, American Society for Composites, Technomic Publishing Co., Lancaster, PA, 1990, pp. 600–610.

[2] Kwon, Y. S. and Sankar, B. V., "Indentation-Flexure Damage in Graphite/Epoxy Laminates," NASA CR 187624, 1991.

[3] Sjöblom, P. O., Hartness, J. T., and Cordell, T. M., "On Low-Velocity Impact Testing of Composite Materials," *Journal of Composite Materials*, Vol. 22, 1988, pp. 30–52.

[4] Sankar, B. V., "Contact Law for Transversely Isotropic Materials," in *Proceedings of the 26th SDM Conference*, AIAA/ASME/ASCE/AHS, Orlando, FL, 1985, pp. 516–521.

[5] Bostaph, G. M. and Elber, W., "Static Indentation Tests on Composite Plates for Impact Susceptibility Evaluation," in *Proceedings of the Army Symposium on Solid Mechanics*, AMMRC MS 82-4, U.S. Army, September 1982, pp. 288–317.

[6] Elber, W., "Failure Mechanics in Low-Velocity Impacts on Thin Composite Plates," NASA Technical Paper 2152, 1983.

[7] Dost, E. F., Ilcewicz, L. B., and Gosse, J. H., "Sublaminate Stability Based Modeling of Impact-Damaged Composite Laminates," in *Proceedings of the 3rd Technical Conference*, American Society for Composites, Seattle, WA, September 1988, pp. 354–363.

[8] Timoshenko, S. and Woinowsky-Krieger, S., *Theory of Plates and Shells*, McGraw-Hill, New York, 1959.

[9] Pinheiro, M. A. S., "Finite Elements for Free Edge Delaminations and Delaminated Anisotropic Beams" Ph.D dissertation, University of Florida, Gainesville, FL, 1991.